

First Measurement of Charged Current Muon Neutrino-Induced K^+ Production on Argon using the MicroBooNE Detector

P. Abratenko,³⁹ D. Andrade Aldana,¹⁴ L. Arellano,²² J. Asaadi,³⁸ A. Ashkenazi,³⁷ S. Balasubramanian,¹² B. Baller,¹² A. Barnard,²⁹ G. Barr,²⁹ D. Barrow,²⁹ J. Barrow,²⁶ V. Basque,¹² J. Bateman,^{15,22} O. Benevides Rodrigues,¹⁴ S. Berkman,²⁵ A. Bhat,⁷ M. Bhattacharya,¹² M. Bishai,³ A. Blake,¹⁹ B. Bogart,²⁴ T. Bolton,¹⁸ M. B. Brunetti,^{17,41} L. Camilleri,¹⁰ D. Caratelli,⁴ F. Cavanna,¹² G. Cerati,¹² A. Chappell,⁴¹ Y. Chen,³³ J. M. Conrad,²³ M. Convery,³³ L. Cooper-Troendle,³⁰ J. I. Crespo-Anadón,⁶ R. Cross,⁴¹ M. Del Tutto,¹² S. R. Dennis,⁵ P. Detje,⁵ R. Diurba,² Z. Djurcic,¹ K. Duffy,²⁹ S. Dytman,³⁰ B. Eberly,³⁵ P. Englezos,³² A. Ereditato,^{7,12} J. J. Evans,²² C. Fang,⁴ G. A. Fiorentini Aguirre,³⁴ W. Foreman,^{14,20} B. T. Fleming,⁷ D. Franco,⁷ A. P. Furmanski,²⁶ F. Gao,⁴ D. Garcia-Gamez,¹³ S. Gardiner,¹² G. Ge,¹⁰ S. Gollapinni,²⁰ E. Gramellini,²² P. Green,²⁹ H. Greenlee,¹² L. Gu,¹⁹ W. Gu,³ R. Guenette,²² P. Guzowski,²² L. Hagaman,⁷ M. D. Handley,⁵ O. Hen,²³ C. Hilgenberg,²⁶ G. A. Horton-Smith,¹⁸ A. Hussain,¹⁸ B. Irwin,²⁶ M. S. Ismail,³⁰ C. James,¹² X. Ji,²⁷ J. H. Jo,³ R. A. Johnson,⁸ D. Kalra,¹⁰ G. Karagiorgi,¹⁰ W. Ketchum,¹² M. Kirby,³ T. Kobilarcik,¹² N. Lane,^{15,22} J.-Y. Li,¹¹ Y. Li,³ K. Lin,³² B. R. Littlejohn,¹⁴ L. Liu,¹² W. C. Louis,²⁰ X. Luo,⁴ T. Mahmud,¹⁹ C. Mariani,⁴⁰ D. Marsden,²² J. Marshall,⁴¹ N. Martinez,¹⁸ D. A. Martinez Caicedo,³⁴ S. Martynenko,³ A. Mastbaum,³² I. Mawby,¹⁹ N. McConkey,³¹ V. Meddage,¹⁸ L. Mellet,²⁵ J. Mendez,²¹ J. Micallef,^{23,39} A. Mogan,⁹ T. Mohayai,¹⁶ M. Mooney,⁹ A. F. Moor,⁵ C. D. Moore,¹² L. Mora Lepin,²² M. M. Moudgalya,²² S. Mulleriababu,² D. Naples,³⁰ A. Navrer-Agasson,¹⁵ N. Nayak,³ M. Nebot-Guinot,¹¹ C. Nguyen,³² J. Nowak,¹⁹ N. Oza,¹⁰ O. Palamara,¹² N. Pallat,²⁶ V. Paolone,³⁰ A. Papadopoulou,¹ V. Papavassiliou,²⁸ H. B. Parkinson,¹¹ S. F. Pate,²⁸ N. Patel,¹⁹ Z. Pavlovic,¹² E. Piasetzky,³⁷ K. Pletcher,²⁵ I. Pophale,¹⁹ X. Qian,³ J. L. Raaf,¹² V. Radeka,³ A. Rafique,¹ M. Reggiani-Guzzo,¹¹ J. Rodriguez Rondon,³⁴ M. Rosenberg,³⁹ M. Ross-Lonergan,²⁰ I. Safa,¹⁰ D. W. Schmitz,⁷ A. Schukraft,¹² W. Seligman,¹⁰ M. H. Shaevitz,¹⁰ R. Sharankova,¹² J. Shi,⁵ E. L. Snider,¹² M. Soderberg,³⁶ S. Söldner-Rembold,¹⁵ J. Spitz,²⁴ M. Stancari,¹² J. St. John,¹² T. Strauss,¹² A. M. Szec, ¹¹ N. Taniuchi,⁵ K. Terao,³³ C. Thorpe,²² D. Torbunov,³ D. Totani,⁴ M. Touns,¹² A. Trettin,²² Y.-T. Tsai,³³ J. Tyler,¹⁸ M. A. Uchida,⁵ T. Usher,³³ B. Viren,³ J. Wang,²⁷ M. Weber,² H. Wei,²¹ A. J. White,⁷ S. Wolbers,¹² T. Wongjirad,³⁹ K. Wresilo,⁵ W. Wu,³⁰ E. Yandel,^{4,20} T. Yang,¹² L. E. Yates,¹² H. W. Yu,³ G. P. Zeller,¹² J. Zennaro,¹² and C. Zhang³

(The MicroBooNE Collaboration)*

¹Argonne National Laboratory (ANL), Lemont, IL, 60439, USA

²Universität Bern, Bern CH-3012, Switzerland

³Brookhaven National Laboratory (BNL), Upton, NY, 11973, USA

⁴University of California, Santa Barbara, CA, 93106, USA

⁵University of Cambridge, Cambridge CB3 0HE, United Kingdom

⁶Centro de Investigaciones Energéticas, Medioambientales y Tecnológicas (CIEMAT), Madrid E-28040, Spain

⁷University of Chicago, Chicago, IL, 60637, USA

⁸University of Cincinnati, Cincinnati, OH, 45221, USA

⁹Colorado State University, Fort Collins, CO, 80523, USA

¹⁰Columbia University, New York, NY, 10027, USA

¹¹University of Edinburgh, Edinburgh EH9 3FD, United Kingdom

¹²Fermi National Accelerator Laboratory (FNAL), Batavia, IL 60510, USA

¹³Universidad de Granada, Granada E-18071, Spain

¹⁴Illinois Institute of Technology (IIT), Chicago, IL 60616, USA

¹⁵Imperial College London, London SW7 2AZ, United Kingdom

¹⁶Indiana University, Bloomington, IN 47405, USA

¹⁷The University of Kansas, Lawrence, KS, 66045, USA

¹⁸Kansas State University (KSU), Manhattan, KS, 66506, USA

¹⁹Lancaster University, Lancaster LA1 4YW, United Kingdom

²⁰Los Alamos National Laboratory (LANL), Los Alamos, NM, 87545, USA

²¹Louisiana State University, Baton Rouge, LA, 70803, USA

²²The University of Manchester, Manchester M13 9PL, United Kingdom

²³Massachusetts Institute of Technology (MIT), Cambridge, MA, 02139, USA

²⁴University of Michigan, Ann Arbor, MI, 48109, USA

²⁵Michigan State University, East Lansing, MI 48824, USA

²⁶University of Minnesota, Minneapolis, MN, 55455, USA

²⁷Nankai University, Nankai District, Tianjin 300071, China

²⁸New Mexico State University (NMSU), Las Cruces, NM, 88003, USA

²⁹University of Oxford, Oxford OX1 3RH, United Kingdom

³⁰University of Pittsburgh, Pittsburgh, PA, 15260, USA

³¹Queen Mary University of London, London E1 4NS, United Kingdom

³²Rutgers University, Piscataway, NJ, 08854, USA

³³SLAC National Accelerator Laboratory, Menlo Park, CA, 94025, USA

³⁴South Dakota School of Mines and Technology (SDSMT), Rapid City, SD, 57701, USA

³⁵University of Southern Maine, Portland, ME, 04104, USA

³⁶Syracuse University, Syracuse, NY, 13244, USA

³⁷Tel Aviv University, Tel Aviv, Israel, 69978

³⁸University of Texas, Arlington, TX, 76019, USA

³⁹Tufts University, Medford, MA, 02155, USA

⁴⁰Center for Neutrino Physics, Virginia Tech, Blacksburg, VA, 24061, USA

⁴¹University of Warwick, Coventry CV4 7AL, United Kingdom

The MicroBooNE experiment is an 85 tonne active mass liquid argon time projection chamber neutrino detector exposed to the on-axis Booster Neutrino Beam (BNB) at Fermilab. One of MicroBooNE's physics goals is the precise measurement of neutrino interactions on argon in the 1 GeV energy regime. Building on the capabilities of the MicroBooNE detector, this analysis identifies K^+ mesons, a key signature for the study of strange particle production in neutrino interactions. This measurement is furthermore valuable for background estimation for future nucleon decay searches and for improved reconstruction and particle identification capabilities in experiments such as the Deep Underground Neutrino Experiment (DUNE). In this letter, we present the first-ever measurement of a flux-integrated cross section for charged-current muon neutrino induced K^+ production on argon nuclei, determined to be 7.93 ± 3.27 (stat.) ± 2.92 (syst.) $\times 10^{-42}$ cm²/nucleon based on an analysis of 6.88×10^{20} protons on target.

Within the Standard Model (SM), the stability of protons is a consequence of the global symmetry that conserves baryon number. However, various Grand Unified Theories (GUTs) predicting baryon number violation through nucleon decay suggest different decay channels, with a preference for $p \rightarrow e^+\pi^0$, with lifetimes ranging from 10^{34} to 10^{39} years [1]. Similarly, the Supersymmetric Grand Unified Theory (SUSY GUT) favors protons decaying via $p \rightarrow \nu K^+$, with lifetimes of 10^{32} to 10^{35} years [2].

Upcoming large long-baseline neutrino oscillation experiments, such as the Deep Underground Neutrino Experiment (DUNE) [3] and Hyper-Kamiokande [4], have the sensitivity to search for proton decay in this range. Cherenkov detector experiments like Super-Kamiokande [5–7] and Hyper-Kamiokande are particularly suited for $p \rightarrow e^+\pi^0$ decay searches. However, for water Cherenkov detectors, the $p \rightarrow \nu K^+$ decay channel needs to be indirectly detected since the momentum of the produced K^+ (339 MeV/c) is below the Cherenkov detection threshold in water (560 MeV/c). Furthermore, backgrounds from atmospheric neutrino interactions, such as the $\nu_\mu n \rightarrow \mu^- K^+ n$ and $\nu p \rightarrow \nu K^+ \Lambda$ channels, are challenging to distinguish in water Cherenkov detectors.

In contrast, liquid argon time projection chambers (LArTPCs) can directly measure kaons that range out and decay by analyzing their unique energy loss (dE/dx) profile. These profiles, along with topological signatures such as distinctive kinks from kaon decay and the high ionization Bragg peak, allow an enhanced kaon identification. All of these topological and calorimetric features are easily measured using the millimeter-precision imaging capabilities of a LArTPC.

The first measurements of charged-current (CC) and neutral-current (NC) kaon production, reported with the Argonne National Laboratory [8] and GARGAMELLE bubble chambers [9] in 1974 and 1975, observed $\mathcal{O}(10)$ events. Later, in the 1980's, the Brookhaven National Laboratory bubble chamber reported $\mathcal{O}(10)$ CC and NC events with strange particle production in neutrino-hydrogen and neutrino-deuterium interactions [10, 11], and the Fermilab bubble chamber reported $\mathcal{O}(10)$ events and a measured cross section for CC neutrino interactions $\nu_\mu + n \rightarrow \mu^- + \Lambda + K^+$ on a deuterium target for energy ranges between 10 GeV and 250 GeV [12]. Most recently, the MINER ν A experiment measured K^+ production in NC and CC modes on a hydrocarbon target, reporting $\mathcal{O}(100)$ and $\mathcal{O}(1000)$ events respectively [13–15]. In addition, MINER ν A reported the first evidence of coherent kaon production [15, 16].

This letter presents the first measurement of the cross section for K^+ production in neutrino interactions on argon nuclei. The signature of the signal events is a CC ν_μ interaction in the presence of a K^+ in the final state with momentum $230 \text{ MeV}/c < p_{K^+} < 2900 \text{ MeV}/c$. The K^+ should decay either to $\mu^+\nu_\mu$ or $\pi^+\pi^0$ which have branching ratios of 63.56% and 20.67%, respectively [17]. This measurement uses MicroBooNE datasets collected between 2016 and 2018 from the on-axis Booster Neutrino Beam (BNB), equivalent to 6.88×10^{20} protons on target (POT).

As the first quantitative measurement of K^+ production on argon nuclei, this analysis will impact nuclear, neutrino, and proton decay research on two fronts. First, it provides background constraints for future nucleon decay experiments. Atmospheric neutrinos can also produce a K^+ along with other particles, mimicking the signature of $p \rightarrow \nu K^+$ decay. Thus, neutrino-induced K^+ production serves as a background for proton decay

* microboone_info@fnal.gov

studies. Second, this measurement provides input to improve neutrino generator models. In the case of bound proton decay, the K^+ is generated within the nucleus and may interact with other nucleons as it escapes. These interactions can decrease the detected momentum of the K^+ in the detector and may also eject nucleons from the nucleus.

Charged-current neutrino-induced K^+ production occurs through three interaction modes: (1) *single kaon production*, where a CC interaction produces a single kaon with a production energy threshold of $E_{\nu_\mu} \geq 0.79$ GeV, and strangeness is not conserved ($|\Delta S| = 1$); (2) *associated kaon production*, where both a kaon and a hyperon are produced, with a threshold of $E_{\nu_\mu} \geq 1.2$ GeV, and strangeness is conserved; and (3) *coherent production*, where only one kaon is produced in the final state, and the target nucleus remains intact after the neutrino interaction.

Figure 1 shows an event candidate of CC ν_μ kaon production recorded in MicroBooNE data. The kaon decays at rest into a 388 MeV energy muon, which subsequently decays into a Michel electron.

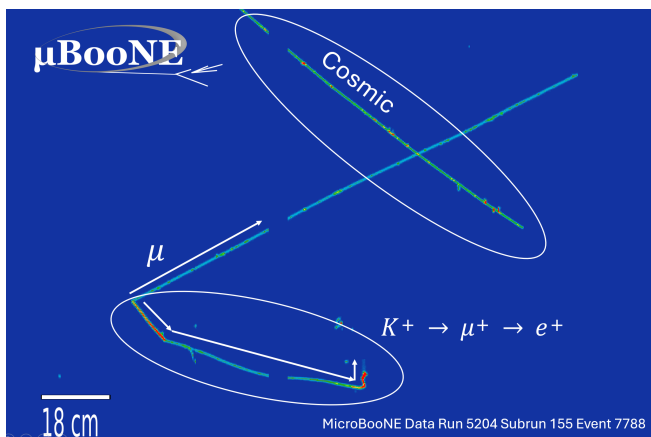


FIG. 1. A $\nu_\mu + \text{Ar} \rightarrow \mu^- + K^+$ interaction candidate observed in MicroBooNE data recorded by the collection plane. The color scale represents the intensity of the ionization charge collected on the TPC wires (green: low intensity, red: high intensity). The x and y-axes represent the wire position in the beam direction and the distance in the drift direction, respectively. The gap shown on each track is due to a region in the detector with no active wires.

The MicroBooNE detector [18, 19] consists of an 85-tonne LArTPC and a photon detection system comprised of 32 photomultiplier tubes (PMTs). The detector identifies neutrino interactions by detecting ionization and scintillation light produced by charged particles moving through the detector. Ionization charge is recorded across three wire planes (two induction, one collection) oriented at different angles (with induction planes at $\pm 60^\circ$ relative to the vertical collection plane). This configuration allows the generation of high-resolution, three-dimensional images of neutrino interactions. Scintillation light collected by the PMTs provides precise

timing information, essential for identifying neutrino interactions that are synchronized with the BNB, and for rejecting cosmic-ray backgrounds.

In MicroBooNE, the LArSoft framework [20] provides tools for simulating the neutrino flux, neutrino interactions, particle propagation, and detector response including ionization and scintillation processes as well as reconstruction of neutrino events. The BNB neutrino flux through the MicroBooNE detector is simulated using the MiniBooNE flux model [21] adapted for MicroBooNE's location along the beamline. GENIE v3.0.6 (G18_10a_02_11a) [22, 23] is the event generator used to simulate neutrino-argon interactions, including both single and associated kaon production. In GENIE, associated kaons are produced via individual resonances simulated by the Rein-Sehgal model [24]. Kaons produced via Deep Inelastic Scattering (DIS) are simulated by the Koba-Nielsen-Olesen (KNO) scaling parameterization [25]. For higher energies (hadronic invariant mass $W > 2.3$ GeV), the AGKY model [26] and PYTHIA6 [27] are used. The hadronization models are tuned to match strange particle production (Λ and K_S^0) observed in experiments such as the Big European Bubble Chamber (BEBC) [28–31] and the Fermilab bubble chamber [32, 33]. The single kaon production model [34] is implemented in GENIE, generating events in the channels $\nu_l + n \rightarrow l^- + n + K^+$, $\nu_l + p \rightarrow l^- + p + K^+$, and $\nu_l + n \rightarrow l^- + p + K^0$. The region of validity assumed for the model is for $E_\nu \leq 2$ GeV [34, 35], while the GENIE authors note that the model can be applied to higher energies as well [36].

Particle trajectories and interactions within the detector are simulated using GEANT4 [37], which models particle propagation in the detector. Simulated neutrino interactions are overlaid with data events collected using an unbiased trigger that operates in anti-coincidence with the beam, enabling data-driven modeling of cosmic ray and detector noise. Both simulation and data reconstruction use the Pandora framework [38], which uses a multi-algorithm approach to pattern recognition and event reconstruction in LArTPCs. Pandora creates clusters from wire hits, identifies the neutrino vertex, matches clusters across wire planes to form 3D objects, classifies reconstructed particles as tracks or showers, and establishes particle hierarchies.

Before performing a dedicated selection for K^+ production signal events, a pre-selection is applied as follows: (1) events must pass a CC inclusive filter which isolates CC neutrino interactions by identifying the presence of an outgoing muon from the vertex of a neutrino interaction [39], (2) all reconstructed tracks in an event must originate within a $2.4 \text{ m} \times 2.1 \text{ m} \times 9.8 \text{ m}$ fiducial volume centered inside the MicroBooNE TPC, and (3) the daughter track (defined as a track connected to the endpoint of one primary signal track candidate) should stop at least 5 cm away from any of the physical edges of the TPC to ensure containment.

For the K^+ event selection, we implemented a boosted

decision tree (BDT) classifier [40]. The BDT classifier inputs include reconstructed variables such as χ^2 values which compare the expected dE/dx for kaon (χ_k^2), proton (χ_p^2), pion (χ_π^2), and muon (χ_μ^2) hypotheses with the observed data for each wire plane, the combined 3-wire-plane χ^2 , the daughter track length, and the log-likelihood ratio particle identification (LLR PID) [41]. We trained the BDT classifier to identify true K^+ that decay to $\mu^+\nu_\mu$ or $\pi^+\pi^0$, using Monte Carlo (MC) simulation samples of reconstructed neutrino interactions that meet the preselection criteria described above. To train the BDT classifier, a background sample corresponding to 3.67×10^{20} POT (equivalent to 10% of the MicroBooNE BNB simulation) was used. For the simulation of the signal, a dedicated high-statistics sample of single and associated K^+ production was used. We optimized the BDT classifier score selection criteria by maximizing the product of efficiency and purity. Figure 2 shows the BDT classifier score distribution, with the orange arrow at 0.41 representing the selected BDT score cut (BDT selection). Events with a score higher than the BDT selection are kept as K^+ candidates, and 10 such K^+ candidates are identified in the data. The total number of background events predicted from the overlay simulation and off-beam data is 2.21 events. The simulation predicts a selection efficiency of 3.95%, and an associated selection purity of 89%. The primary background category for K^+ candidates consists of protons generated at the neutrino vertex that interact with an argon nucleus, producing secondary particles at the proton endpoint that could mimic a K^+ decay product, consisting of 2.08 events.

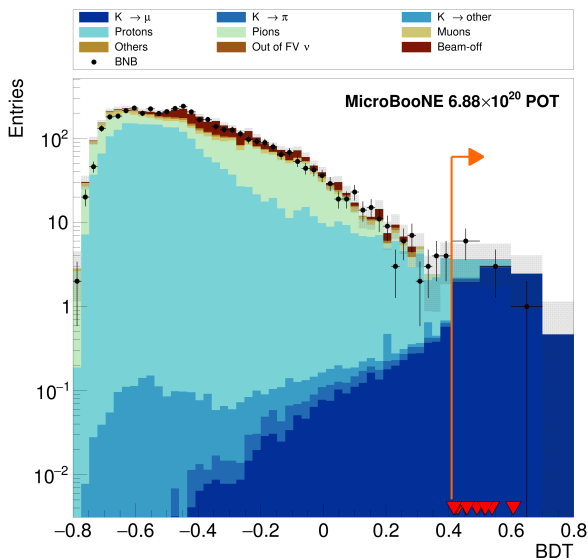


FIG. 2. BDT classifier score distribution. The black dots represent the MicroBooNE data. The stacked histogram represents the expected BDT distribution from the simulation with its statistical uncertainty (gray band). The orange arrow represents the BDT event selection cut. The red triangles are the K^+ candidates selected in MicroBooNE data by the BDT.

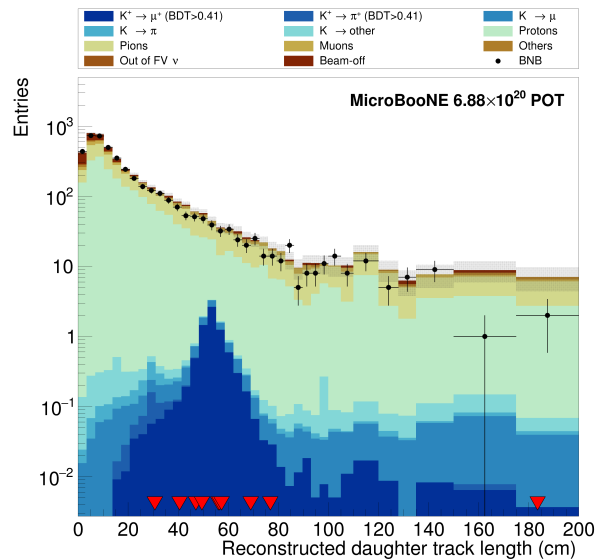


FIG. 3. Reconstructed daughter track length distribution. The stacked histogram shows the MC simulation with its statistical uncertainty (gray band). The black dots represent the MicroBooNE data. The red triangles are the K^+ candidates selected in MicroBooNE data by the BDT.

Figure 3 shows the reconstructed daughter track length distribution of the K^+ candidates selected in MicroBooNE data, including the event shown in Fig. 1. The stacked histogram shows the expected daughter track length distribution from the MicroBooNE BNB simulation. Due to the two-body decay nature of the K^+ branching ratios analyzed in this letter, the resulting mono-energetic μ^+ (π^+) provides a powerful discriminant, as it leads to a fixed track length that can be measured with high accuracy and is not present in background events. The expected track length for μ^+ and π^+ accumulates around 53 cm and 30 cm, respectively. The K^+ candidates selected by the BDT selection in Fig. 3 (red triangles) exhibit a pile-up in the region compatible with K^+ decay.

To evaluate the accuracy of the background modeling, two sideband regions were defined using a 2-dimensional distribution of the BDT classifier score versus daughter track length. A far sideband region is defined to include tracks with low BDT classifier scores ($\text{BDT} < 0$) and track lengths less than 40 cm. A near sideband region selects tracks with BDT classifier scores close to the signal region ($\text{BDT} < 0.41$) and across all track length ranges, but excludes tracks in the far sideband region. The data/MC comparisons of the near and far sidebands show agreement within uncertainties for the reconstructed kinematic variables such as K^+ candidate track length, ϕ (azimuthal angle around the beam direction), and θ (angle of the track with respect to the beam direction). The agreement with the data suggests that the simulation is able to adequately model the background in the cross section extraction. More information about the sideband

comparisons is provided in the Supplemental Material [42].

This analysis presents the measurement of the single-bin flux-integrated cross section for $\nu_\mu + \text{Ar} \rightarrow \mu^- + K^+ + X$ interactions, where muon neutrinos interact with Ar and produce one μ^- , one K^+ and X (any number of other hadrons in the final state) on argon nuclei. This measurement uses an exposure of 6.88×10^{20} POT from the on-axis BNB neutrino beam. The cross section (σ) was found to be 7.93 ± 3.27 (stat.) ± 2.92 (syst.) $10^{-42} \text{cm}^2/\text{nucleon}$, and it was calculated using the following expression:

$$\sigma = \frac{N - B}{\varepsilon \times N_{\text{target}} \times \Phi_{\nu_\mu}}, \quad (1)$$

where N represents the number of selected signal events (10), B is the number of expected background events (2.21), ε is the selection efficiency (3.95%), N_{target} is the number of target nucleons (4.13×10^{31}), and Φ_{ν_μ} stands for the integrated BNB ν_μ flux ($6.02 \times 10^{11} \nu/\text{cm}^2$). The selection efficiency accounts for all possible K^+ decays within the fiducial volume, while the BDT selection identifies K^+ candidates that could decay into either μ^+ or π^+ .

The systematic uncertainties in the measured cross section are evaluated by reweighting and generating simulated events to account for each source of uncertainty [43–45]. For the detector-related uncertainties, a dedicated simulation is used to model the variation in detector responses. In contrast, uncertainties from neutrino interactions and BNB flux modeling are treated with a similar reweighting technique. To evaluate the uncertainty associated with kaon reinteractions within the detector, we implement a methodology similar to that presented by MINER ν A [13]. For each selected K^+ candidate track, a weight W_{inel} is calculated using the following expression to estimate the kaon inelastic reinteraction uncertainty:

$$W_{\text{inel}} = \frac{1 - e^{-\rho x \sigma_{\text{var}}^{\text{tot}}}}{1 - e^{-\rho x \sigma_{\text{geant}}^{\text{tot}}}} \times \frac{\sigma_{\text{var}}^{\text{inel}}}{\sigma_{\text{var}}^{\text{tot}}} \times \frac{\sigma_{\text{geant}}^{\text{tot}}}{\sigma_{\text{geant}}^{\text{inel}}}, \quad (2)$$

where ρ is the density of the material, x is the track length, $\sigma_{\text{geant}}^{\text{tot}}$ and $\sigma_{\text{geant}}^{\text{inel}}$ are the K^+ total and inelastic GEANT4 cross sections, and $\sigma_{\text{var}}^{\text{tot}}$ and $\sigma_{\text{var}}^{\text{inel}}$ are the K^+ total and inelastic cross sections estimated by applying a variation of $\pm 40\%$ to the $\sigma_{\text{geant}}^{\text{inel}}$. The 40% variation covers the disagreement between data and GEANT4 in $K^+ - \text{Ar}$ interaction measurements reported by the LArIAT experiment [46], as well as the disagreement between $K^+ - \text{Ca}$ interaction data and the GEANT4 interaction model [42].

The leading source of systematic uncertainty comes from the detector response (30.3%), with a major contribution from modeling ion recombination of electrons with argon. This analysis relies heavily on identifying

the stopping K^+ and μ^+ (π^+) signatures through their Bragg peak, which itself depends on the charge profile of the track in a highly ionizing regime. Because of this, the mismodeling of ion recombination, which alters the calorimetry in the detector, plays a particularly large role in the total error budget for the measurement. The modeling of neutrino interactions, the BNB neutrino flux, and particle reinteractions in the detector, including kaon inelastic interactions, lead to systematic uncertainties of 12.1%, 11.7%, and 10.4% respectively. The effect of statistics in the estimation of the selection efficiency (6.1%), the number of target nuclei N_{target} (1%), simulation statistical uncertainty (7.4%), and POT exposure (2%) are the remaining sources of uncertainty. The overall magnitude of the uncertainty (statistical and systematic) on our measurement is 55.3%, where the major contribution is due to the statistical uncertainty, with a reported value of 41.3%. Table 1 presents the measured cross section of the $\nu_\mu + \text{Ar} \rightarrow \mu^- + K^+ + X$ interactions and the predictions obtained from various neutrino event generators.

| Generator | cross section ($10^{-42} \text{cm}^2/\text{nucleon}$) |
|------------------------|---|
| GENIE v2.12.10 | 8.67 |
| GENIE v3.00.06 | 8.42 |
| NEUT 5.4.0.1 | 9.71 |
| NuWro 19.02.1 | 10.87 |
| MicroBooNE Data | 7.93 ± 3.27 (stat.) ± 2.92 (syst.) |

TABLE I. The $\nu_\mu + \text{Ar} \rightarrow \mu^- + K^+ + X$ cross section extracted from different neutrino event generators compared with the cross section extracted from data.

The flux-integrated cross section measurement reported in this paper indicates consistency with the predictions from different neutrino event generators, although the large uncertainties prevent a stringent test of these models. The cross section predicted by the NuWro generator [47] is the largest among the generator predictions, but is still within the 1σ uncertainty of the data result.

In conclusion, this letter presents the first measurement of the $\nu_\mu + \text{Ar} \rightarrow \mu^- + K^+ + X$ cross section on argon, using the MicroBooNE dataset collected from the BNB flux with a POT of 6.88×10^{20} . The results reported here represent a significant step forward for future studies aiming to refine background estimates for proton decay searches, particularly within the framework of GUTs and SUSY. To advance this analysis in future LArTPC measurements, it is necessary to increase statistics, reduce large detector systematics (especially those related to the recombination of electrons with argon nuclei), refine reconstruction algorithms for short tracks, and improve the identification of kaon tracks that undergo reinteractions. Furthermore, the uncertainty related to kaon reinteractions on argon nuclei could be refined by using data from LArIAT [46], and the DUNE prototypes at CERN [48]. More statistics will come from analyzing MicroBooNE’s full dataset with a total

of 1.2×10^{21} POT. The future DUNE near detector data could also provide more accurate measurements of CC neutrino-induced K^+ production on argon nuclei enabling improved comparisons among the neutrino generator models. These high-precision measurements will enhance our understanding of rare neutrino interactions and final state interaction modeling, and will improve the background predictions for future nucleon decay searches at DUNE, which currently rely on model predictions.

This document was prepared by the MicroBooNE collaboration using the resources of the Fermi National Accelerator Laboratory (Fermilab), a U.S. Department of Energy, Office of Science, Office of High Energy Physics HEP User Facility. Fermilab is managed by Fermi Forward Discovery Group, LLC, acting under Contract No. 89243024CSC000002. MicroBooNE is supported by the following: the U.S. Department of Energy, Office of Science, Offices of High Energy Physics and Nuclear Physics; the U.S. National Science Foundation; the

Swiss National Science Foundation; the Science and Technology Facilities Council (STFC), part of the United Kingdom Research and Innovation; the Royal Society (United Kingdom); the UK Research and Innovation (UKRI) Future Leaders Fellowship; and the NSF AI Institute for Artificial Intelligence and Fundamental Interactions. Additional support for the laser calibration system and cosmic ray tagger was provided by the Albert Einstein Center for Fundamental Physics, Bern, Switzerland. We also acknowledge the contributions of technical and scientific staff to the design, construction, and operation of the MicroBooNE detector as well as the contributions of past collaborators to the development of MicroBooNE analyses, without whom this work would not have been possible. For the purpose of open access, the authors have applied a Creative Commons Attribution (CC BY) public copyright license to any Author Accepted Manuscript version arising from this submission.

-
- [1] H. Georgi and S. L. Glashow, “Unity of All Elementary-Particle Forces,” *Phys. Rev. Lett.* **32**, 438–441 (1974).
- [2] J. Hisano, H. Murayama, and T. Yanagida, “Nucleon decay in the minimal supersymmetric SU(5) grand unification,” *Nucl. Phys. B* **402**, 46–84 (1993), arXiv:hep-ph/9207279.
- [3] B. Abi *et al.*, “Deep Underground Neutrino Experiment (DUNE), Far Detector Technical Design Report, Volume I. Introduction to DUNE,” *J. Instrum.* **15**, T08008 (2020).
- [4] K. Abe *et al.* (Super-Kamiokande Collaboration), “Hyper-Kamiokande Design Report,” (2018), arXiv:1805.04163 [physics.ins-det].
- [5] K. Abe *et al.* (Super-Kamiokande Collaboration), “Search for proton decay via $p \rightarrow \nu K^+$ using 260 kiloton · year data of Super-Kamiokande,” *Phys. Rev. D* **90**, 072005 (2014).
- [6] K. Abe *et al.* (Super-Kamiokande Collaboration), “Search for proton decay via $p \rightarrow e^+ \pi^0$ and $p \rightarrow \mu^+ \pi^0$ in 0.31 megaton · years exposure of the Super-Kamiokande water Cherenkov detector,” *Phys. Rev. D* **95**, 012004 (2017).
- [7] K. Abe *et al.* (Super-Kamiokande Collaboration), “Search for proton decay via $p \rightarrow e^+ \pi^0$ and $p \rightarrow \mu^+ \pi^0$ with an enlarged fiducial volume in Super-Kamiokande I-IV,” *Phys. Rev. D* **102**, 112011 (2020).
- [8] S. J. Barish *et al.*, “Strange-Particle Production in Neutrino Interactions,” *Phys. Rev. Lett.* **33**, 1446–1449 (1974).
- [9] H. Deden *et al.*, “Strange particle production and charmed particle search in the Gargamelle neutrino experiment,” *Phys. Lett., B*, v. 58, no. 3, pp. 361–366 (1975), 10.1016/0370-2693(75)90674-7.
- [10] J. E. Jensen, “THE BROOKHAVEN NATIONAL LABORATORY 80-INCH LIQUID HYDROGEN BUBBLE CHAMBER,” in *1964 Cryogenic Engineering Conference* (1964).
- [11] N. J. Baker *et al.*, “Strange-particle production from neutrino interactions in the BNL 7-foot bubble chamber,” *Phys. Rev. D* **24**, 2779–2786 (1981).
- [12] D. Son *et al.*, “Quasielastic charmed-baryon production and exclusive strange-particle production by high-energy neutrinos,” *Phys. Rev. D* **28**, 2129–2134 (1983).
- [13] C. M. Marshall *et al.* (MINER ν A Collaboration), “Measurement of K^+ production in charged-current ν_μ interactions,” *Phys. Rev. D* **94**, 012002 (2016).
- [14] C. M. Marshall *et al.* (MINER ν A Collaboration), “Measurement of Neutral-Current K^+ Production by Neutrinos using MINER ν A,” *Phys. Rev. Lett.* **119**, 011802 (2017).
- [15] C. M. Marshall, *Measurement of charged kaon production by neutrinos at MINER ν A*, Ph.D. thesis, U. Rochester (2016).
- [16] Z. Wang, C. M. Marshall, *et al.* (MINER ν A Collaboration), “Evidence of Coherent K^+ Meson Production in Neutrino-Nucleus Scattering,” *Phys. Rev. Lett.* **117**, 061802 (2016).
- [17] S. Navas *et al.* (Particle Data Group Collaboration), “Review of Particle Physics,” *Phys. Rev. D* **110**, 030001 (2024).
- [18] B. Fleming (MicroBooNE Collaboration), “The MicroBooNE Technical Design Report,” (2012), 10.2172/1333130.
- [19] R. Acciarri *et al.* (MicroBooNE Collaboration), “Design and Construction of the MicroBooNE Detector,” *JINST* **12**, P02017 (2017), arXiv:1612.05824 [physics.ins-det].
- [20] E. L. Snider and G. Petrillo, “LArSoft: Toolkit for Simulation, Reconstruction and Analysis of Liquid Argon TPC Neutrino Detectors,” *J. Phys. Conf. Ser.* **898**, 042057 (2017).
- [21] A. A. Aguilar-Arevalo *et al.* (MiniBooNE Collaboration), “Neutrino flux prediction at MiniBooNE,” *Phys. Rev. D* **79**, 072002 (2009).
- [22] C. Andreopoulos *et al.*, “The GENIE Neutrino Monte Carlo Generator,” *Nucl. Instrum. Meth. A* **614**, 87–104 (2010), arXiv:0905.2517 [hep-ph].
- [23] C. Andreopoulos *et al.* (GENIE Collaboration), “Neutrino-nucleon cross-section model tuning in GENIE

- v3,” Phys. Rev. D **104**, 072009 (2021).
- [24] D. Rein and L. M. Sehgal, “Neutrino-excitation of baryon resonances and single pion production,” Annals of Physics **133**, 79–153 (1981).
- [25] Z. Koba, H.B. Nielsen, and P. Olesen, “Scaling of multiplicity distributions in high energy hadron collisions,” Nucl. Phys. B **40**, 317–334 (1972).
- [26] T. Yang, C. Andreopoulos, H. Gallagher, K. Hofmann, and P. Kehayias, “A hadronization model for few-GeV neutrino interactions,” Eur. Phys. J. C **63**, 1–10 (2009).
- [27] T. Sjöstrand, S. Mrenna, and P. Skands, “PYTHIA 6.4 physics and manual,” J. High Energy Phys. **2006**, 026–026 (2006).
- [28] G. T. Jones *et al.*, “Neutral strange particle production in neutrino and anti-neutrino charged current interactions on protons,” Z. Phys. C **57**, 197–210 (1993).
- [29] D. Allasia *et al.*, “Production of neutral strange particles in $\nu_\mu d_2$ and $\bar{\nu}_\mu d_2$ charged current interactions,” Nucl. Phys. B **224**, 1–20 (1983).
- [30] S. Willocq *et al.* (WA59 Collaboration), “Neutral strange particle production in anti-neutrino - neon charged current interactions,” Z. Phys. C **53**, 207–218 (1992).
- [31] P. Bosetti *et al.*, “Strange particle production in ν and $\bar{\nu}$ neon interactions,” Nucl. Phys. B **209**, 29–44 (1982).
- [32] N. J. Baker *et al.*, “Strange-particle production in neutrino-neon charged-current interactions,” Phys. Rev. D **34**, 1251–1264 (1986).
- [33] D. DeProspero *et al.*, “Neutral strange particle production in neutrino and antineutrino charged-current interactions on neon,” Phys. Rev. D **50**, 6691–6703 (1994).
- [34] M. Rafi Alam, I. Ruiz Simo, M. Sajjad Athar, and M. J. Vicente Vacas, “Weak kaon production off the nucleon,” Phys. Rev. D **82**, 033001 (2010).
- [35] L. Alvarez-Ruso, J. Nieves, I. Ruiz Simo, M. Valverde, and M. J. Vicente Vacas, “Charged kaon production by coherent scattering of neutrinos and antineutrinos on nuclei,” Phys. Rev. C **87**, 015503 (2013).
- [36] M. Alam, C. Andreopoulos, *et al.*, “GENIE Production Release 2.10.0,” (2015), arXiv:1512.06882 [hep-ph].
- [37] S. Agostinelli *et al.*, “Geant4 — a simulation toolkit,” Nucl. Instrum. Meth. A **506**, 250–303 (2003).
- [38] R. Acciarri *et al.*, “The Pandora multi-algorithm approach to automated pattern recognition of cosmic-ray muon and neutrino events in the MicroBooNE detector,” Eur. Phys. J. C **78** (2018), 10.1140/epjc/s10052-017-5481-6.
- [39] P. Abratenko *et al.* (MicroBooNE), “First Measurement of Inclusive Muon Neutrino Charged Current Differential Cross Sections on Argon at $E_\nu \sim 0.8$ GeV with the MicroBooNE Detector,” Phys. Rev. Lett. **123**, 131801 (2019), arXiv:1905.09694 [hep-ex].
- [40] A. Hoecker *et al.*, “TMVA - Toolkit for Multivariate Data Analysis,” (2009), arXiv:physics/0703039 [physics.data-an].
- [41] P. Abratenko *et al.* (MicroBooNE Collaboration), “Calorimetric classification of track-like signatures in liquid argon TPCs using MicroBooNE data,” J. High Energy Phys. **2021** (2021), 10.1007/jhep12(2021)153.
- [42] Supplemental Material.
- [43] J. Calcutt, C. Thorpe, K. Mahn, and L. Fields, “Geant4Reweight: a framework for evaluating and propagating hadronic interaction uncertainties in Geant4,” J. Instrum. **16**, P08042 (2021).
- [44] P. Abratenko *et al.* (MicroBooNE Collaboration), “Novel approach for evaluating detector-related uncertainties in a LArTPC using MicroBooNE data,” Eur. Phys. J. C **82** (2022), 10.1140/epjc/s10052-022-10270-8.
- [45] The MicroBooNE Collaboration, “Neutrino Interaction Model and Uncertainties for MicroBooNE Analyses,” MicroBooNE Public Note, MICROBOONE-NOTE-1074-PUB (2020).
- [46] E. Gramellini, *Measurement of the Negative Pion and Positive Kaon Total Hadronic Cross Sections on Argon at the LArIAT Experiment*, Ph.D. thesis, Yale U. (2018).
- [47] T. Golan, J.T. Sobczyk, and J. Żmuda, “NuWro: the Wrocław Monte Carlo Generator of Neutrino Interactions,” Nucl. Phys. B - Proc. Suppl. **229-232**, 499 (2012), Neutrino 2010.
- [48] A. Abed Abud *et al.* (DUNE Collaboration), “First measurement of the total inelastic cross section of positively charged kaons on argon at energies between 5.0 and 7.5 GeV,” Phys. Rev. D **110**, 092011 (2024).